HHS Public Access

Author manuscript

Nat Neurosci. Author manuscript; available in PMC 2010 May 01.

Published in final edited form as:

Nat Neurosci. 2009 November ; 12(11): 1424–1430. doi:10.1038/nn.2404.

Functional consequences of animal-to-animal variation in circuit parameters

Jean-Marc Goaillard[*], **Adam L. Taylor**, **David J. Schulz**[§], and **Eve Marder**

Volen Center and Biology Department Brandeis University Waltham, MA 02454-9100 USA

[§]Biological Sciences, University of Missouri at Columbia, Columbia, Missouri 65211, USA

Abstract

How different are the neuronal circuits for a given behavior across individual animals? To address this question, we measured multiple cellular and synaptic parameters within individual preparations to see how they correlate with circuit function, using neurons and synapses within the pyloric circuit of the stomatogastric ganglion (STG) of the crab *Cancer borealis*. There was considerable preparation-to-preparation variability in the strength of two identified synapses, in the amplitude of a modulator-evoked current, and in the expression of six ion channel genes. Nonetheless, across preparations we found strong correlations among these parameters and attributes of circuit performance. These data illustrate the importance of making multidimensional measurements from single preparations to understand how variability in circuit output is related to the variability of multiple circuit parameters.

INTRODUCTION

How tightly tuned do synaptic strengths and intrinsic membrane conductances need to be for a neuronal circuit to perform adequately? Theoretical work has shown that similar circuit performance can result from appreciably different sets of synaptic strengths and ionic conductance densities1–4. These studies suggest that if one were to look across a population of healthy adult animals, one might find substantial variability in synaptic strength and ion channel number, even in the same identified neuron. Moreover, recent experimental studies have found that membrane currents and synaptic strengths can vary several-fold across individual neurons of the same cell type2,5–9. Additionally, there can be significant correlations between the conductances of voltage-gated currents10, and between the genes that code for different channels7,11.

How does variability in cellular and synaptic parameters relate to variability at the level of circuit function? We approached this question by measuring multiple cellular/synaptic

Please address all correspondence to: Dr. J-M Goaillard. goaillard@univmed.fr.

[*]present address: INSERM UMR 641, Faculté de Médecine - Secteur Nord, Université de la Méditerranée, CS80011, Bd Pierre Dramard, 13344 MARSEILLE Cedex 15, FRANCE

Author contributions: JMG conducted the majority of the electrophysiological experiments, analyzed data, and contributed to writing the manuscript; ALT analyzed data, conducted experiments, and contributed to writing the manuscript; DJS performed all quantitative single-cell PCR; EM supervised the experiments and contributed to writing the manuscript.

parameters in each preparation to see how they correlated with circuit function, using neurons and synapses within the pyloric circuit of the stomatogastric ganglion (STG) of the crab *Cancer borealis*12.

Some of these results might have been predicted from our current understanding of how the pyloric circuit works13–15, but others are counterintuitive. This study makes clear the importance of collecting as much data as possible on individual preparations, rather than relying on studies of circuit parameters measured one-by-one in separate experiments.

RESULTS

The pyloric circuit (Supplementary Fig. 1) generates a rhythmic pattern of activity that drives contractions of the pylorus, part of the crab stomach12. The pyloric rhythm consists of a triphasic motor pattern in which the pyloric dilator (PD), lateral pyloric (LP) and pyloric (PY) neurons sequentially fire bursts of action potentials (Fig. 1a) to coordinate pyloric contractions16.

Variability of the output of the pyloric circuit

Figure 1 characterizes the variability of the pyloric motor patterns recorded from 69 animals. For each animal, we recorded 137 cycles (~2 min) of the ongoing pyloric rhythm using extracellular recordings (Fig. 1a). For each pyloric cycle, we measured the period and the timing of burst onset and offset for each of the three pyloric phases. By convention, the onset of the PD burst is considered the start of each pyloric cycle, and the other onset/offset times are measured as the delay from the start of the cycle to the first/last spike of a burst. In this way, we measured PD offset, LP onset, LP offset, PY onset, and PY offset for each cycle (Fig. 1a). The pyloric period was variable from animal to animal: pyloric periods ranged from 0.53 s to 1.44 s, with a coefficient of variation of 18.8% (mean: 0.90 s, SD: 0.17 s; coefficient of variation is SD/mean, which we report as a percentage; Fig. 1b). The pyloric period in each animal was stable from cycle to cycle: the maximum value of the coefficient of variation was 2.6%, and the mean coefficient of variation was 1.5% (Fig 1b, inset).

Burst onset and offset delays scaled with pyloric period (Fig. 1c). The linear regression lines for each burst onset/offset passed through the origin (y-intercept not significantly different from zero, $P>0.18$ for all burst events), indicating that each delay was proportional to pyloric period. Dividing delay by period gives the phase of each burst event; phase was independent of period (Fig. 1d, slopes not significantly different from zero, $P>0.15$ for all burst events), as implied by the result that delay scaled with period. The mean phase of each burst event was consistent from animal to animal; PY onset showed the highest variability, with an SD equal to 0.050 cycles.

Burst durations were proportional to period (Fig. 1e; y-intercept not significantly different from zero, $P>0.18$ for all bursts), as burst onsets and offsets both scaled with period.

In each crab, there are two PD neurons, three to five PY neurons, but only one LP neuron. The presence of multiple individual neurons on each pyloric dilator nerve (*pdn*) and pyloric

nerve (*pyn*) nerve made it difficult to extract spike rates for individual neurons. Because there is a single LP neuron, it is easy to measure the LP interspike interval (ISI) within the burst (Fig. 1f). The ISI of LP scaled with pyloric period (*y*-intercept not significantly different from zero, P=0.26). That LP burst duration and ISI both scaled with period implies that the number of LP spikes in the burst does not vary with period, as was the case (data not shown; slope not significantly different from zero, P=0.45).

Variability of pacemaker synaptic inputs to LP

The firing properties of the crab LP neuron have been extensively studied17,18, making the LP neuron an ideal choice for studying the relationship between synaptic/cellular properties and circuit function.

We first examined the variability of synaptic inputs to the LP neuron. The anterior burster (AB) neuron and the two PD neurons form an electrically-coupled “pacemaker kernel” that rhythmically inhibits the LP neuron (Fig. 2a and Supplementary Fig. 1). The AB neuron is glutamatergic and elicits a fast inhibitory post-synaptic potential (IPSP) in LP with a reversal potential of about −70 mV, while the PD neurons are cholinergic and evoke a slower IPSP with a reversal potential of about −90 mV19,20. The AB and PD neurons depolarize and fire almost synchronously, and they evoke a composite IPSP in LP with variable contributions from the two classes of presynaptic neurons19,20. Because the LP neuron fires on rebound from the synaptic inhibition it receives from the pacemaker kernel (Fig. 2a and Supplementary Fig. 1), we analyzed the properties of the composite inhibitory post-synaptic current (IPSC) from the AB/PD neurons and then dissociated the composite IPSC into its components from the AB and PD neurons (Methods).

To record synaptic currents, we voltage-clamped the LP neuron during the ongoing pyloric rhythm, and stepped it to potentials from −120 mV to −60 mV. (This changed the pyloric period only slightly, because the pyloric frequency is mainly determined by the intrinsic frequency of the pacemaker kernel, which is the primary driver of oscillatory activity in the pyloric network21–24.) Simultaneously, we recorded extracellular PD spikes from the *pdn* (as in Fig. 1a) to monitor the phase of the pyloric rhythm. In one typical experiment, the IPSC was outward at −60 mV, was close to reversal at −80 mV, and was clearly inward at −90 mV (Fig. 2b). This reflects a composite reversal potential between that of the AB synapse (~ −70 mV) and that of the PD synapse (~ −90 mV).

There was a high degree of variability in the amplitudes and reversal potentials of the IPSCs across preparations. To quantify this, we isolated the synaptic current from other currents by finding the phase of the pyloric cycle with the lowest conductance and subtracting this nonsynaptic conductance from the total conductance to get the synaptic conductance (Methods). The resulting composite IPSCs displayed a wide range of reversal potentials (Fig. 2c). Reversal potentials were quantified by constructing I–V curves of the synaptic current at peak conductance (Methods), and ranged from −85.2 mV to −72.7 mV (Fig. 2d).

Taking advantage of the difference in reversal potentials of the AB- and PD-evoked IPSCs, we decomposed the composite IPSCs into AB- and PD-derived components (Methods). Preparations with hyperpolarized composite reversal potentials had relatively large PD-

evoked synaptic conductances and small AB-evoked synaptic conductances, while those with depolarized composite reversal potentials had large AB-evoked synaptic conductances and small PD-evoked synaptic conductances (Fig. 2e). Consequently, AB- and PD-evoked synaptic conductances showed opposite correlations with the value of the composite reversal potential (slope=7.8±1.4 nS/mV and −6.7±0.7 nS/mV, respectively; $P<0.001$; ± gives standard error, here and elsewhere). This was also reflected in the negative correlation between the AB-evoked conductance and the PD-evoked conductance ($r=-0.46$, $P<0.05$, $n=22$). The composite synaptic conductance was not correlated with the value of the composite reversal potential (Fig. 2e; slope=1.1±2.1 nS/mV, $P=0.61$). All of these quantities displayed substantial variability (Fig. 2e): the coefficient of variation of the composite synaptic conductance was 18.9% (mean: 154 nS, SD: 29 nS), and the SD of the composite reversal potential was 3.1 mV (mean=−77.5 mV). For the individual synaptic components, the coefficient of variation of the AB synaptic conductance was 32.5% (mean: 97 nS, SD: 32 nS), and that of the PD synaptic conductance was 40.5% (mean: 57 nS, SD: 23 nS).

Variability of a modulator-activated current in LP

The pacemaker kernel neurons and the LP neuron are modulated by a large number of amines and neuropeptides12,25 that influence their excitability (Supplementary Fig. 1). Among these is the neuropeptide crustacean cardioactive peptide (CCAP), which activates a voltage-dependent inward current26–28 called the modulator-activated inward current (I_{MI}). CCAP, acting on I_{MI}, strongly modulates the frequency and phasing of the pyloric rhythm29. I_{MI} has a bell-shaped steady-state I–V curve that makes it sensitive to changes in voltage between −60 mV and −20 mV, and it shows little inactivation.

We compared the variability in I_{MI} with the variability of the synaptic currents, and looked for correlations between them, and between them and the pyloric circuit output. Therefore, we measured I_{MI} in LP neurons by voltage-clamping and ramping the command potential from −95 mV to 0 mV (135 mV/s), both in control saline and while puffing on 10^{-4} M CCAP (Fig. 3a, top panel). (Experiments were done in the presence of blockers to eliminate other voltage-gated currents that might have contaminated the measurements of I_{MI}, and to eliminate endogenous sources of neuromodulators; Methods.) I_{MI} was obtained by subtraction of the current measured before application from the current measured during application of the peptide (Fig. 3a, middle panel). The I–V curve obtained was then fit to an equation describing the theoretical steady-state I–V of I_{MI} (Methods). Two parameters were extracted to characterize I_{MI}: the peak current and the voltage at peak current (Fig. 3a, bottom panel). These were variable (Fig. 3b); the coefficient of variation of the peak current was 38.6% (mean: 3.19 nA, SD: 1.23 nA), and the SD of the voltage at peak current was 7.7 mV (mean: −13.78 mV). There was no significant correlation between the peak current and the voltage at peak current ($r=0.31$, $P=0.27$).

Correlations among synaptic currents, I_{MI}, and LP firing

We next looked for correlations between the measured properties of the synaptic currents, I_{MI}, and circuit performance (Fig. 4). There was a strong positive correlation between the PD synaptic conductance and the phase of LP onset (LP-on phase; Fig. 4a). In contrast, we found a negative and weaker correlation between the AB synaptic conductance and the LP-

on phase (Fig. 4b). The LP-on phase was also positively correlated with the magnitude of the peak I_{MI} (Fig. 4c). As expected from the above, we found a positive correlation between the magnitude of the peak I_{MI} and the PD synaptic conductance (Fig. 4d).

Correlations among IH, shal, *and LP firing*

Because the LP and PY neurons fire on rebound from inhibition, the dependence of their firing phase on the hyperpolarization-activated inward current (I_H) and the transient outward current (I_A) has been extensively studied10,14,15,30. Over-expression of the mRNA encoding I_A causes an increase in I_H10,30, and I_H and I_A mRNA expressions are highly correlated in individual LP neurons of *C. borealis* across animals7,11. Consequently, we asked how mRNA expression for these channel genes correlated with circuit output. In 11 experiments, we measured the mRNA levels of six channel subunits after physiological recordings: *shal* (I_A), *IH* (I_H), *shab* (a delayed-rectifier potassium current), *shaw* (a different delayed-rectifier potassium current), *para* (the fast sodium channel), and *BKKCa* (a calcium-dependent potassium current)11. (Each mRNA codes for a subunit of the channel in parentheses.) In the LP neuron, there was no significant correlation between *IH* copy number and LP-on phase (Fig. 5a, top left). Nor was there a significant correlation between *shal* copy number and LP-on phase (Fig. 5a, top right). But the copy number of both genes was significantly correlated with LP-on delay (Fig. 5a, bottom). The expression levels of these two genes were also significantly correlated with LP mean ISI and with pyloric period (Fig. 5b, left; Table 1), but failed to show a significant correlation with LP burst duration (Fig. 5b, right; *shal*: r=0.16, P=0.637, n=11).

Pyloric period was strongly correlated with LP-on delay, LP mean ISI and LP burst duration (Fig. 1, Table 1). Additionally, the expression levels of *IH*, *shal*, *shaw* and *shab* are strongly correlated with one another in LP7,11. Therefore, we looked for correlations between the level of expression of these channels and LP firing properties. The expression of the *shaw* channel had a significant correlation with LP-on delay and LP mean ISI (Table 1), but not with pyloric period (r=0.54, P=0.111, n=10) or LP burst duration (r=0.06, P=0.878, n=10). *Shab* expression was significantly correlated with LP mean ISI (Table 1) but not with other firing parameters, such as pyloric period (r=0.52, P=0.126, n=10), LP-on delay (r=0.57, P=0.0824, n=10), and LP burst duration (r=0.23, P=0.523, n=10).

shal *expression level in PD scales with pyloric period*

The PD neurons are part of the pacemaker kernel. Because I_H and I_A are important for burst properties in many systems9,31, we asked whether the expression of *IH* and *shal* in the PD neurons might be correlated with the pyloric period.

The two PDs from the same animal show very similar levels of expression for both *IH* and *shal*7. This similarity becomes a problem when studying correlations between a circuit property (pyloric period) and the expression levels in two PD cells from the same preparation. The PD neurons were from eight animals, five with data from two PD neurons, three with data from one PD neuron. When calculating correlations, we arbitrarily picked a single PD neuron from those with measurements for both. We repeated this process 32 ($=2^5$)

times, once for each possible combination. Thus each correlation was calculated from data on eight PD neurons, one from each preparation.

IH expression was significantly correlated with pyloric period for only 25% of the 32 combinations ($0.50 \leq r \leq 0.83$, $\alpha=0.05$, $n=8$; Fig. 5c, left), while *shal* levels were significantly correlated with pyloric period for all combinations ($0.82 \leq r \leq 0.96$, $\alpha=0.05$, $n=8$; Fig. 5c, right). In contrast, *BKKCa* expression did not show a significant correlation with pyloric period, even when all PD neurons (including paired PDs) were included ($r=0.25$, $P=0.41$, $n=13$). *BKKCa* expression was nonetheless strongly correlated with *shal* expression ($r=0.92$, $P<0.01$, $n=8$). In summary, only the *shal* expression level in PD was significantly correlated with pyloric period.

DISCUSSION

The crabs used in this paper had spent years foraging for food in the cold waters of the Atlantic Ocean before being trapped by fishermen. As such, they were all successful survivors of the vagaries of their sometimes inhospitable natural environment, and thus by definition their nervous systems were “good enough” for them to feed, grow, and molt. Consequently, the variability we document here is likely to be a representative sample of the natural population, with its disparate genetic make-ups and life histories. Differences in both genetic make-up and life history could lead to variability in synaptic strengths, voltage-gated channel densities, and baseline neuromodulator/ hormonal concentrations.

Previous work on voltage-dependent currents and the expression of the mRNA encoding them in crabs showed animal-to-animal variability in the same identified neurons of 2–4-fold2,6,7, and similarly variable levels of conductances in neurons of the same type in genetically identical mice5,8. We now report several-fold animal-to-animal variability of the conductances of identified synapses, similar to that seen at identified synapses in the leech heartbeat system32,33. Additionally, the I_{MI} modulatory conductance was highly variable across animals, with almost a 6-fold range in its amplitude, and considerable variation in its voltage-dependence.

Our data on pyloric circuit output show 2–3-fold variability in pyloric period across animals, but also show that many aspects of pyloric output scale with period, and thus are phase constant (Fig. 1). These results agree with similar results on the American lobster, *Homarus americanus*34. We found relatively little variability in the pyloric rhythm from cycle to cycle (Fig. 1b, inset; Fig. 1c–e, error bars). This contrasts with feeding behavior in *Aplysia californica*, which exhibits substantial cycle-to-cycle variability, and where the question of “how good is good enough” has been raised in a different context35.

When studying animal-to-animal variability, it is essential to establish that one is not simply observing variability caused by measurement error. Two observations indicate that measurement error cannot account for most of the variability observed here. First, the mRNA levels measured in the electrically coupled PD neurons from a single animal showed much less variation than that found in PD neurons from different animals7. Second, the

strong correlations presented here and previously7,11 argue strongly that much of the variability is true animal-to-animal variation.

Thus there are two remaining explanations of the several-fold variability in neuronal and network parameters measured here and previously5,7,11,32,33. The variability could occur because the value of a given parameter is not critical for the performance of the system. For example, once an inhibitory synaptic input to an oscillatory neuron is strong enough, increasing it further may have no impact on the oscillator's behavior23,35. Or, the variability could be accompanied by compensatory covariation of other parameters, that would induce correlations among different parameters. To understand how important a given parameter is for system function, one must know which of these possibilities accounts for the measured variation across individuals. The answer to this question has important implications for understanding the mechanisms by which synaptic strength and intrinsic properties are regulated.

In this paper, we related circuit performance to multiple underlying parameters by looking at variability and correlations between the two. More commonly, attempts to connect an intrinsic or synaptic current to a neuron's firing have experimentally perturbed a single parameter at a time. For example, the dynamic clamp is often used to alter the parameters of a single current to determine how the firing properties of a neuron or a network are influenced by that current35–37. This is similar to a conventional sensitivity analysis in theoretical studies18. These start with an individual, and look at the effects of changing a single parameter on system behavior. In contrast, the approach taken here starts with a natural population, and asks whether there are correlations among any of the parameters and system behaviors. To our knowledge, something similar has been done only once before, and was limited to examining the relationship between I_A current density, the mRNAs that code for I_A channel subunits, and spontaneous spike rate, the last of which was found to be negatively correlated with the first two in substantia nigra dopaminergic neurons8.

In the present study, we found several correlations among intrinsic, synaptic, and functional properties, in both PD and LP neurons (Supplementary Fig. 2). The strongest correlation between PD parameters and circuit output was between *shal* expression and pyloric period (Supplementary Fig. 2a), which makes intuitive sense because I_A acts to delay burst onset15,38.

In the LP neuron, the expression levels of *IH*, *shal*, *shab*, and *shaw* form a nested “Venn diagram” of correlations with different network properties (Supplementary Fig. 2b). All are correlated with one another, and all are correlated with the ISI of the LP neuron. *IH*, *shab*, and *shaw* expression are correlated with the LP-on delay. *IH* and *shal* are strongly correlated with the pyloric period. Thus both the PD and LP's *shal* expression are correlated with the overall period.

There was a strong correlation between the strength of the PD-evoked synaptic current and the amplitude of I_{MI}, and high values of these imply a later phase of LP burst onset (Supplementary Fig. 2c). A similar relationship between the strength of the slow IPSP evoked by the PD neuron and the phase of follower neuron firing was seen previously when

the strength of the synapse was varied13. This is an example in which single parameter manipulations and the examination of correlations across animals give congruent results. Both results make sense because the synapses from the PD neurons are slower and longer-lasting than those from the AB neuron19,20, so they play a larger role in determining the burst onset in follower neurons. In contrast to our results, others report a negative correlation between IPSP amplitude and LP-on phase, for the IPSPs from both AB and PD onto LP, in the spiny lobster *Panulirus interruptus*39. The apparent contradiction between our results and theirs could result from the difference in species or in experimental design.

At first glance the strong correlation between I_{MI} and LP-on phase is counterintuitive, as one would expect that increasing I_{MI} would advance LP phase by making LP more excitable21,27,28. However, because there appear to be strong pressures for the pyloric rhythm to remain phase constant (Fig. 1), it is possible that the strength of the PD synapse onto LP and I_{MI} are coordinately regulated so that the increase in I_{MI} partially, but incompletely, compensates for the effects of increasing the strength of the PD to LP synapse.

All of these interactions can be summarized as a “network” of correlations, in which various intrinsic and synaptic properties of the pyloric circuit are correlated with one another, and with particular circuit output properties (Supplementary Fig. 2d).

Interestingly, our data provide evidence that synaptic inputs from different neurons might be regulated in a coordinated manner to reach a specific functional output: AB and PD conductances are significantly negatively correlated, such that the total conductance is held approximately constant (Fig. 2e).

LP's channel mRNAs seem to correlate more strongly with LP's single-cell firing properties than with more circuit-level properties. In particular, four mRNA species correlated with LP ISI, three correlated with LP-on delay, and only two with pyloric period. This may reflect the fact that ISI during the burst is mainly set by LP's intrinsic properties, the delay is set partly by intrinsic properties and partly by the properties of other cells and synapses in the circuit, and the period is even more dependent on factors extrinsic to LP. Additionally, it is noteworthy that the intrinsic currents in LP are correlated with quantities measured in units of time (ISI, LP-on delay, period), but the synaptic and MI currents are correlated with the *phase* of LP-on (i.e. delay normalized by period). It is interesting to speculate that different regulatory schemes might be required for the homeostatic control of delays versus phases. According to this hypothesis, *IH*, *shal*, *shab* and *shaw* would belong to one regulatory subnetwork while the synaptic conductances and the MI current would belong to a different one.

Despite the apparent logic of the relationships observed (Supplementary Fig. 2), the existence of correlations does not imply that these correlations are necessary for the function of the network, as some correlations among ion channels or receptors could be a consequence of developmental or transcriptional processing, but not be strictly required for the production of dynamics. This possibility was underscored by a recent computational study of a population of LP neuron models, which failed to show strong correlations

between LP parameters, even though the models were constrained to behave like biological LP cells18.

Studies on non-neuronal systems show that genetically identical cells or animals show significant variability in many underlying cellular parameters, and that variable solutions to the production of similar phenotypes are an important substrate for evolutionary selection40,41. Although it is tempting to think that brain circuits are optimally designed, a large body of work suggests that there are many “good enough” solutions consistent with the normal behavior of healthy animals in their usual environments. These solutions will be accompanied by variable sets of network parameters, and the challenge is to discover new experimental strategies, such as the multidimensional measurements used here, that can assess which neuronal and circuit elements are variable but functionally critical, and which are only loosely controlled, as they are less essential for the animal's behavior.

METHODS

Adult *Cancer borealis* crabs were obtained from Commercial Lobster (Boston, MA) and maintained in artificial seawater until used. Crabs were anesthetized by keeping them on ice for 30 min before dissection. The complete stomatogastric nervous system, consisting of the paired commisural ganglia, the esophageal ganglion, the STG, and some of the motor nerves, was dissected out of the animal and pinned out in a Sylgard-coated (Dow Corning, Midland MI) dish containing chilled (9–13 °C) saline. The physiological saline solution consisted of the following (in mM) : NaCl, 440; KCl, 11; $CaCl_2$, 13; $MgCl_2$, 26; Trizma base, 11; and maleic acid, 5; pH,7.45.

Quantitative Single-Cell RT-PCR

Data on the expression levels of *IH*, *shal*, *shaw*, and *shab* mRNA presented here (Fig. 5, Table 1) were described previously11. Physiological analysis of these experiments and correlation of mRNA levels with firing pattern were performed specifically for the present publication.

Electrophysiological recordings

For electrophysiological recordings, the STG was desheathed, and petroleum jelly wells were placed on the motor nerves. Extracellular recordings from the nerves were made by placing stainless steel pin electrodes in the wells. Signals were amplified and filtered using a differential AC amplifier (A–M Systems, Carlsborg WA). Intracellular recordings from the STG somata were made using 20–40 MΩ glass microelectrodes, filled with 0.6 M K_2SO_4 and 20 mM KCl, and an Axoclamp 2A amplifier (Axon Instruments, Union City CA). Pyloric motor neurons were identified using standard procedures for *C. borealis*42,43. During recording, the preparation was continuously superfused with chilled (9–13 °C) physiological saline.

For control recordings of the ongoing pyloric rhythm (Fig. 1), 137 cycles (~2 min) of the pyloric rhythm were recorded from each animal. All STNSs used for these recordings had two intact superior esophageal nerves (*sons)*, but they varied in the number of intact inferior esophageal nerves (*ions)*. Of the 69 control animals, 47 had two *ion*s (mean

period=0.88±0.02, SD=0.16±0.03), 13 had one *ion* (mean period=0.97±0.06, SD=0.21±0.04), and 12 had zero *ion*s (mean period=0.95±0.04, SD=0.14±0.03). These differences in mean period, though suggestive, did not achieve statistical significance, using either one-way ANOVA (P=0.15) or the Kruskal-Wallis test (P=0.10), and the standard deviations show that there was substantial overlap between the three populations. Control recordings were used only if there was no visible nonstationarity (a slow trend) or gastric modulation in the sequence of 137 cycles, either in the period or the delays to burst onset/offset. We took the first/last spike of each burst on the *pdn* recording (from either PD neuron) as the PD burst onset/offset, and used the first/last spike of each burst on the *pyn* recording (from any PY neuron) as the burst onset/offset. Because the timing of the last spike during the LP burst is far more variable than the timing of the other spikes, the last spike was not included in calculations of mean ISI.

The ongoing pyloric rhythm (Figs. 1, 4, 5) was recorded extracellularly before any neuron was impaled with microelectrodes.

Synaptic current recordings and analysis

To record synaptic currents, the LP neuron was voltage-clamped and stepped to hyperpolarized potentials ranging from −60 mV to −120 mV during the ongoing pyloric rhythm. Extracellular PD spikes were recorded from the pyloric dilator nerve (*pdn*) to monitor the ongoing pyloric rhythm (Fig. 2b). Synaptic currents were measured in control saline to preserve spontaneous pyloric activity, and they were always measured before the PD cells were impaled. For larger hyperpolarizations, a noticeable I_H developed after several pyloric cycles. I_H activates quite slowly in *C. borealis*: the smallest time constant over the range of voltages used is >5 s17,44. To minimize contamination of synaptic current measurements by I_H, only the first three cycles after the start of the hyperpolarizing step were analyzed. Each time sample of each synaptic current recording was assigned a corresponding pyloric phase using the recording of PD spikes (Supplementary Fig. 3). By convention, the onset of the PD burst was defined to have a phase of zero (Fig. 2b). Phase was then binned into 100 bins, and all current samples within the same phase bin were averaged together. We then computed the I–V curve for each phase bin (Supplementary Fig. 3a, top middle), and fit a line to each I–V curve (Supplementary Fig. 3a, top right). For these fits, we only used voltages between −95 mV and −75 mV, to prevent contamination by voltage-activated currents. The slope of each of these lines gives the total conductance for that phase bin. We assumed that the minimum conductance represented the nonsynaptic conductance, and subtracted out the nonsynaptic I–V curve to determine the synaptic current at each phase and voltage (Supplementary Fig. 3a, bottom left and middle). (If there is baseline synaptic release even at the minimum-conductance point, then our measure would be the synaptic conductance that varies over a pyloric cycle.) A linear fit of the synaptic I–V curve was performed at each phase (Supplementary Fig. 3a, bottom right). The slope of each line gives the total conductance of the synaptic input at that phase, and the x-intercept (the voltage at which the current is zero) gives the composite reversal potential. These were then plotted versus the pyloric phase (Supplementary Fig. 3b). These plots were used to determine the maximum composite synaptic conductance (Max gABPD in Table 1, Supplementary Fig. 3), the phase at which this maximum occurred (Phase of Max gABPD in

Table 1), and the composite reversal potential at this phase (Erev in Table 1, Supplementary Fig. 3; see also Fig. 2 for data on all these quantities).

The synaptic conductance at each phase is the sum of the synaptic conductance from the AB cell (glutamatergic) and that from the PD cells (cholinergic)20. Because the synaptic input from the AB cell reverses at −70 mV, and that from the PD cells reverses at −90 mV20, the synaptic I–V curve at each phase can be used to estimate both the AB and PD conductance at that phase. This was done using a nonnegative least squares regression to the synaptic I–V curve, for voltages from −95 mV to −75 mV. This regression determined the AB and PD conductances that provided the best fit to the synaptic I–V curve, subject to the constraint that conductances be nonnegative. Because of uncertainty about the precise reversal potentials, several combinations of values for AB and PD reversal potentials were used (−70/−90, −70/−85, −65/−85). While modifying reversal potentials changed somewhat the relative contribution of AB and PD to the synaptic input, the main results of the study (weak correlation between AB conductance and LP-on phase, strong correlation between PD conductance and LP-on phase, strong correlation between PD conductance and MI current, Fig. 4) were insensitive to these changes. Therefore, we used the values of −70 mV and −90 mV in results shown here. It is reassuring that the PD synaptic component extracted in this way generally outlasts that of AB (Fig. 4b, bottom; note that PD component is generally larger for phases from +0.25 to +0.5), consistent with the PD synapse being slower than that of AB20,39.

MI current recordings and analysis

For I_{MI} measurements, voltage-activated and synaptic currents were blocked by adding 0.1 μM tetrodotoxin (TTX; Alomone Laboratories, Jerusalem, Israel), 10 μM picrotoxin (PTX; Sigma, St Louis MO; PTX blocks glutamatergic transmission in *C. borealis*) and 10 mM tetraethylammonium chloride (TEA; Sigma) to the bath saline. I_{MI} was elicited using long-lasting puff applications (10–20 s) of CCAP (Bachem, Torrance CA) at saturating concentration (100 μM) using a Picospritzer (General Valve Corporation, Fairfield NJ). Although I_{MI} is activated by many peptides26,27, CCAP was used because it generally produces larger responses in the LP neuron than other agonists. CCAP acts hormonally on the STG12, so all the preparations studied here were deprived of endogenous CCAP for approximately two hours before the MI current was measured, presumably minimizing any variability in the recorded current caused by variability in receptor desensitization. Furthermore, most nonhormonal neuromodulators released onto STG neurons are released from the terminals of axonal projections from other ganglia, and all or most of this release is blocked by the presence of TTX, which blocks spikes in these axons12. Variability in the state of second messenger pathways mediating the CCAP response may be reflected in our measurements. I_{MI} was measured by applying voltage ramps (−95 to 0 mV, 135 mV/s) to the cell in control saline and during CCAP application, and subtracting control ramp current from CCAP ramp current (Fig. 3a). I_{MI} I–V curves were fit by the equation

$$i(\nu) = i_0 + \bar{g}\,\frac{1}{1+exp\left[-\left(\nu-\nu_{half}\right)/s\right]}\left(\nu - e_{rev}\right), \quad (1)$$

where i_0 is basal current, $\bar{g}$ is the maximal conductance of the current, v is voltage, v_{half} is half-activation voltage, *s* scales the voltage-sensitivity of activation, and e_{rev} is the reversal potential of the current.

Data acquisition and analysis

Data were acquired using a Digidata 1200 data acquisition board (Axon Instruments) and subsequently analyzed in Clampfit (version 9; Axon Instruments), Matlab (version R2006b; The Mathworks, Natick MA) and Spike2 (version 4; Cambridge Electronic Design, Cambridge, UK). Analyzed data were plotted using SigmaPlot (version 10; Systat Software, San Jose CA), and statistical tests were performed in SigmaStat (version 3.5; Systat Software, San Jose CA). Sample correlation coefficients were calculated in the usual way, and tested for significance using a *t* test. They were considered to be significant for P-values < 0.05. Final figure composition was done in Adobe Illustrator 10 (Adobe Systems, Mountain View CA).

Supplementary Material

Refer to Web version on PubMed Central for supplementary material.

ACKNOWLEDGEMENTS

We thank Stefan R. Pulver and Lamont S. Tang for contributing data to Figure 1. This work was supported by National Institutes of Health Grants NS17813 (EM), MH46742 (EM), and NS50928 (ALT); James S. McDonnell Foundation Grant 220020065 (EM); and National Science Foundation Grant IOB-0615160 (DJS).

REFERENCES

1. Prinz AA, Bucher D, Marder E. Similar network activity from disparate circuit parameters. Nat Neurosci. 2004; 7:1345–1352. [PubMed: 15558066]
2. Goldman MS, Golowasch J, Marder E, Abbott LF. Global structure, robustness, and modulation of neuronal models. J. Neurosci. 2001; 21:5229–5238. [PubMed: 11438598]
3. Achard P, De Schutter E. Complex parameter landscape for a complex neuron model. PLoS Comput Biol. 2006; 2:e94. [PubMed: 16848639]
4. Marder E, Goaillard JM. Variability, compensation and homeostasis in neuron and network function. Nat Rev Neurosci. 2006; 7:563–574. [PubMed: 16791145]
5. Swensen AM, Bean BP. Robustness of burst firing in dissociated purkinje neurons with acute or long-term reductions in sodium conductance. J Neurosci. 2005; 25:3509–3520. [PubMed: 15814781]
6. Golowasch J, Abbott LF, Marder E. Activity-dependent regulation of potassium currents in an identified neuron of the stomatogastric ganglion of the crab *Cancer borealis*. J. Neurosci. 1999; 19:RC33. [PubMed: 10516335]
7. Schulz DJ, Goaillard JM, Marder E. Variable channel expression in identified single and electrically coupled neurons in different animals. Nat Neurosci. 2006; 9:356–362. [PubMed: 16444270]
8. Liss B, et al. Tuning pacemaker frequency of individual dopaminergic neurons by Kv4.3L and KChip3.1 transcription. Embo J. 2001; 20:5715–5724. [PubMed: 11598014]
9. Liss B, Roeper J. Correlating function and gene expression of individual basal ganglia neurons. Trends Neurosci. 2004; 27:475–481. [PubMed: 15271495]
10. MacLean JN, et al. Activity-independent coregulation of I_A and I_h in rhythmically active neurons. J Neurophysiol. 2005; 94:3601–3617. [PubMed: 16049145]

11. Schulz DJ, Goaillard JM, Marder EE. Quantitative expression profiling of identified neurons reveals cell-specific constraints on highly variable levels of gene expression. Proc Natl Acad Sci U S A. 2007; 104:13187–13191. [PubMed: 17652510]
12. Marder E, Bucher D. Understanding circuit dynamics using the stomatogastric nervous system of lobsters and crabs. Annu Rev Physiol. 2007; 69:291–316. [PubMed: 17009928]
13. Eisen JS, Marder E. A mechanism for production of phase shifts in a pattern generator. J. Neurophysiol. 1984; 51:1375–1393. [PubMed: 6145759]
14. Harris-Warrick RM, Coniglio LM, Barazangi N, Guckenheimer J, Gueron S. Dopamine modulation of transient potassium current evokes phase shifts in a central pattern generator network. J. Neurosci. 1995; 15:342–358. [PubMed: 7823140]
15. Harris-Warrick RM, Coniglio LM, Levini RM, Gueron S, Guckenheimer J. Dopamine modulation of two subthreshold currents produces phase shifts in activity of an identified motoneuron. J. Neurophysiol. 1995; 74:1404–1420. [PubMed: 8989381]
16. Thuma JB, Harness PI, Koehnle TJ, Morris LG, Hooper SL. Muscle anatomy is a primary determinant of muscle relaxation dynamics in the lobster (*Panulirus interruptus*) stomatogastric system. J Comp Physiol A Neuroethol Sens Neural Behav Physiol. 2007; 193:1101–1113. [PubMed: 17710408]
17. Golowasch J, Marder E. Ionic currents of the lateral pyloric neuron of the stomatogastric ganglion of the crab. J. Neurophysiol. 1992; 67:318–331. [PubMed: 1373762]
18. Taylor AL, Goaillard JM, Marder E. How multiple conductances determine electrophysiological properties in a multicompartmental model. J Neurosci. 2009; 29:5573–5586. [PubMed: 19403824]
19. Eisen JS, Marder E. Mechanisms underlying pattern generation in lobster stomatogastric ganglion as determined by selective inactivation of identified neurons. III. Synaptic connections of electrically coupled pyloric neurons. J. Neurophysiol. 1982; 48:1392–1415. [PubMed: 6296329]
20. Marder E, Eisen JS. Transmitter identification of pyloric neurons: electrically coupled neurons use different neurotransmitters. J. Neurophysiol. 1984; 51:1345–1361. [PubMed: 6145757]
21. Hooper SL, Marder E. Modulation of the lobster pyloric rhythm by the peptide proctolin. J. Neurosci. 1987; 7:2097–2112. [PubMed: 3612231]
22. Miller, JP. Pyloric Mechanisms. In: Selverston, AI.; Moulins, M., editors. The Crustacean Stomatogastric System. Springer-Verlag; Berlin: 1987.
23. Thirumalai V, Prinz AA, Johnson CD, Marder E. Red pigment concentrating hormone strongly enhances the strength of the feedback to the pyloric rhythm oscillator but has little effect on pyloric rhythm period. J Neurophysiol. 2006; 95:1762–1770. [PubMed: 16319213]
24. Nadim F, Manor Y, Kopell N, Marder E. Synaptic depression creates a switch that controls the frequency of an oscillatory circuit. Proc Natl Acad Sci U S A. 1999; 96:8206–8211. [PubMed: 10393973]
25. Nusbaum MP, Blitz DM, Swensen AM, Wood D, Marder E. The roles of co-transmission in neural network modulation. Trends Neurosci. 2001; 24:146–154. [PubMed: 11182454]
26. Swensen AM, Marder E. Multiple peptides converge to activate the same voltage-dependent current in a central pattern-generating circuit. J Neurosci. 2000; 20:6752–6759. [PubMed: 10995818]
27. Swensen AM, Marder E. Modulators with convergent cellular actions elicit distinct circuit outputs. J. Neurosci. 2001; 21:4050–4058. [PubMed: 11356892]
28. Golowasch J, Marder E. Proctolin activates an inward current whose voltage dependence is modified by extracellular Ca^{2+} J. Neurosci. 1992; 12:810–817. [PubMed: 1347561]
29. Weimann JM, et al. Modulation of oscillator interactions in the crab stomatogastric ganglion by crustacean cardioactive peptide. J. Neurosci. 1997; 17:1748–1760. [PubMed: 9030633]
30. MacLean JN, Zhang Y, Johnson BR, Harris-Warrick RM. Activity-independent homeostasis in rhythmically active neurons. Neuron. 2003; 37:109–120. [PubMed: 12526777]
31. Luthi A, McCormick DA. H-current: properties of a neuronal and network pacemaker. Neuron. 1998; 21:9–12. [PubMed: 9697847]
32. Norris BJ, Weaver AL, Wenning A, Garcia PS, Calabrese RL. A central pattern generator producing alternative outputs: pattern, strength, and dynamics of premotor synaptic input to leech heart motor neurons. J Neurophysiol. 2007; 98:2992–3005. [PubMed: 17804574]

33. Norris BJ, Weaver AL, Wenning A, Garcia PS, Calabrese RL. A central pattern generator producing alternative outputs: phase relations of leech heart motor neurons with respect to premotor synaptic input. J Neurophysiol. 2007; 98:2983–2991. [PubMed: 17728387]
34. Bucher D, Prinz AA, Marder E. Animal-to-animal variability in motor pattern production in adults and during growth. J Neurosci. 2005; 25:1611–1619. [PubMed: 15716396]
35. Prinz AA, Thirumalai V, Marder E. The functional consequences of changes in the strength and duration of synaptic inputs to oscillatory neurons. J. Neurosci. 2003; 23:943–954. [PubMed: 12574423]
36. van Welie I, van Hooft JA, Wadman WJ. Homeostatic scaling of neuronal excitability by synaptic modulation of somatic hyperpolarization-activated I_h channels. Proc Natl Acad Sci U S A. 2004; 101:5123–5128. [PubMed: 15051886]
37. Lien CC, Jonas P. Kv3 potassium conductance is necessary and kinetically optimized for high-frequency action potential generation in hippocampal interneurons. J. Neurosci. 2003; 23:2058–2068. [PubMed: 12657664]
38. Tierney AJ, Harris-Warrick RM. Physiological role of the transient potassium current in the pyloric circuit of the lobster stomatogastric ganglion. J. Neurophysiol. 1992; 67:599–609. [PubMed: 1578246]
39. Rabbah P, Nadim F. Distinct synaptic dynamics of heterogeneous pacemaker neurons in an oscillatory network. J Neurophysiol. 2007; 97:2239–2253. [PubMed: 17202242]
40. Greenspan RJ. The flexible genome. Nat Rev Genet. 2001; 2:383–387. [PubMed: 11331904]
41. Chouard T. Darwin 200: Beneath the surface. Nature. 2008; 456:300–303. [PubMed: 19020592]
42. Hooper SL, et al. The innervation of the pyloric region of the crab, *Cancer borealis*: homologous muscles in decapod species are differently innervated. J. Comp. Physiol. A. 1986; 159:227–240. [PubMed: 2876096]
43. Weimann JM, Meyrand P, Marder E. Neurons that form multiple pattern generators: identification and multiple activity patterns of gastric/pyloric neurons in the crab stomatogastric system. J. Neurophysiol. 1991; 65:111–122. [PubMed: 1999725]
44. Buchholtz F, Golowasch J, Epstein IR, Marder E. Mathematical model of an identified stomatogastric ganglion neuron. J. Neurophysiol. 1992; 67:332–340. [PubMed: 1373763]

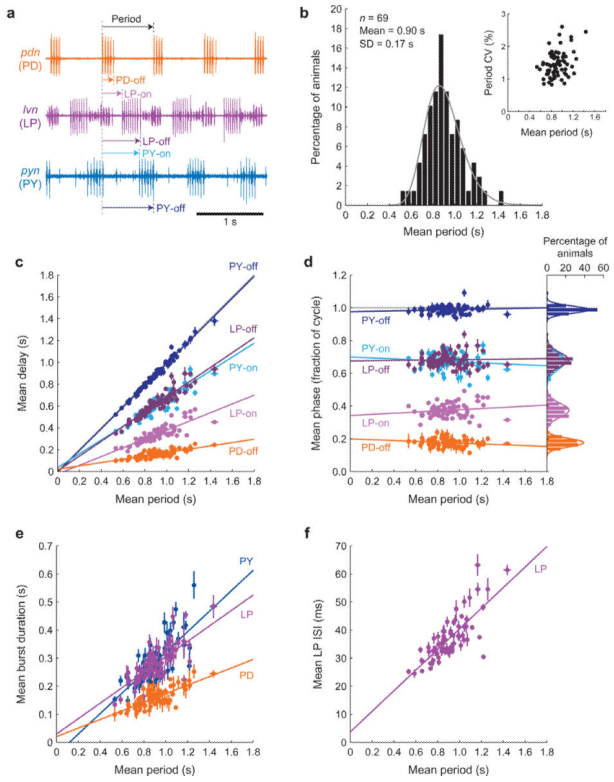

Figure 1.

Variability of pyloric circuit output across animals. **(a)** Typical extracellular recordings of pyloric neurons. Simultaneous recordings from the pyloric dilator nerve (*pdn)*, lateral ventricular nerve (*lvn)*, and pyloric nerve (*pyn)*. The large spikes in the *pdn/lvn/pyn* recording are from the PD/LP/PY neurons. The various measurements of a single cycle (see text) are illustrated by the arrows. **(b)** Histogram showing distribution of mean pyloric period for ganglia from 69 animals. The smooth curve is a lognormal distribution (used because the data cannot be negative, and the histogram is asymmetric) fit to the data. The inset shows the coefficient of variation (CV) of the pyloric period for each animal, plotted versus the mean period for that animal. **(c)** Mean delay versus mean period for each animal. For each event type (PD-off, LP-on, LP-off, PY-on, PY-off), the mean delay is plotted versus mean period, for each animal. Colors for each event type match those in **a**. In all panels, error bars represent SDs (but are sometimes smaller than the symbols). Lines are linear fits for each event type. Gray line (largely obscured by PY-off fit line) is the identity line. **(d)** Mean phase versus mean period for each animal. Similar conventions to **c** were used. Inset shows histograms of mean phase for each event type. Smooth curves are normal distributions fit to each data set. **(e)** Mean PD/LP/PY burst duration versus mean period for each animal, with fits. **(f)** Mean LP interspike interval (ISI) versus mean period for each animal, with fit.

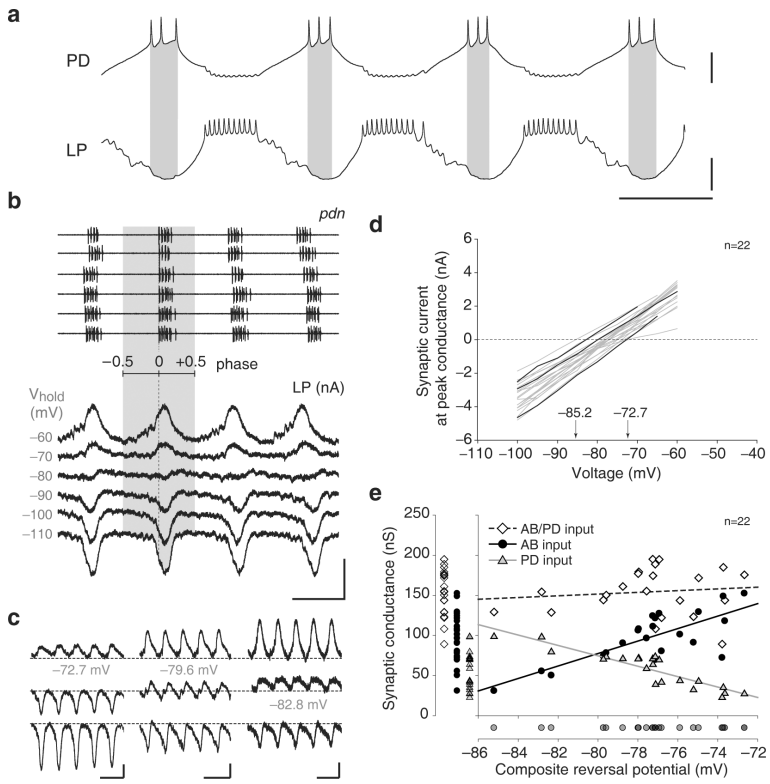

Figure 2.

Variability of synaptic inputs to LP. **(a)** Simultaneous intracellular recordings of the PD and LP neurons. Gray shading shows the pronounced hyperpolarization of LP voltage during PD activity. Vertical scale bars: −60 to −40 mV, horizontal scale bar: 500 ms. Synaptic currents recorded in LP during ongoing pyloric activity. **(b)** Extracellular PD recordings (top traces) were used to align synaptic current traces (bottom traces). Vertical scale bar: 5 nA, horizontal scale bar: 500 ms. **(c)** Raw synaptic currents in three preparations with different composite reversal potentials (gray numbers). Traces are from holding potentials of −70, −80, and −90 mV. Black dotted lines represent zero current. Vertical scale bars: 2 nA, horizontal scale bar: 1 s. **(d)** Raw I–V curves of synaptic current after subtraction of nonsynaptic current (*n*=22). Black lines correspond to the recordings shown in panel **c**. Arrows indicate the minimum and maximum values of composite synaptic reversal potential observed across all preparations. **(e)** Plot showing the relationship between maximal synaptic conductance (composite, AB, and PD) and composite reversal potential. Data points are projected onto the *x*- and *y*-axes to show the range of values displayed by the four variables shown.

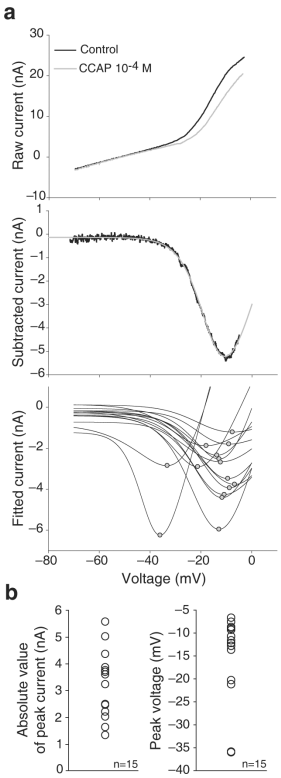

Figure 3.

Variability of I_{MI} in LP. (**a**) Measurement of I_{MI} I–V curves. Top: ramp currents recorded in control condition (black line) and in the presence of 10^{-4} M CCAP (gray line). Middle: I_{MI} obtained by subtraction of the control ramp current from the CCAP ramp current (black line). Gray line is the fit obtained using Equation 1, in Methods. Bottom: fits of I_{MI} obtained from 15 different preparations. Gray circles indicate peak current. **(b)** Variability in amplitude and voltage of peak I_{MI}.

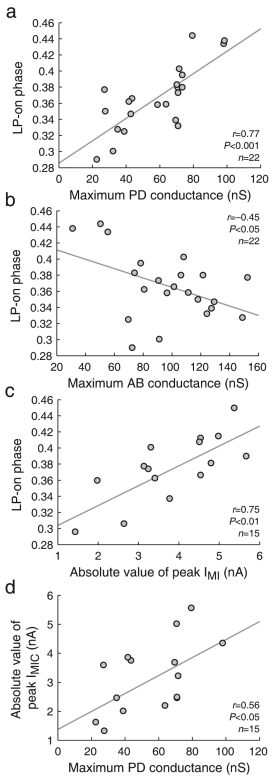

Figure 4.

Correlations among synaptic current properties, I_{MI}, and LP firing properties. **(a)** LP-on phase was significantly correlated with maximum PD conductance. In all panels, gray line is a linear fit with *x* as the independent variable, *r* is the sample correlation coefficient, and P-value is from a test of the null hypothesis that the true correlation coefficient is zero (see Methods). **(b)** LP-on phase was significantly correlated with maximum AB conductance. **(c)** LP-on phase was significantly correlated with I_{MI} peak current amplitude. **(d)** I_{MI} peak current amplitude was significantly correlated with maximum PD conductance.

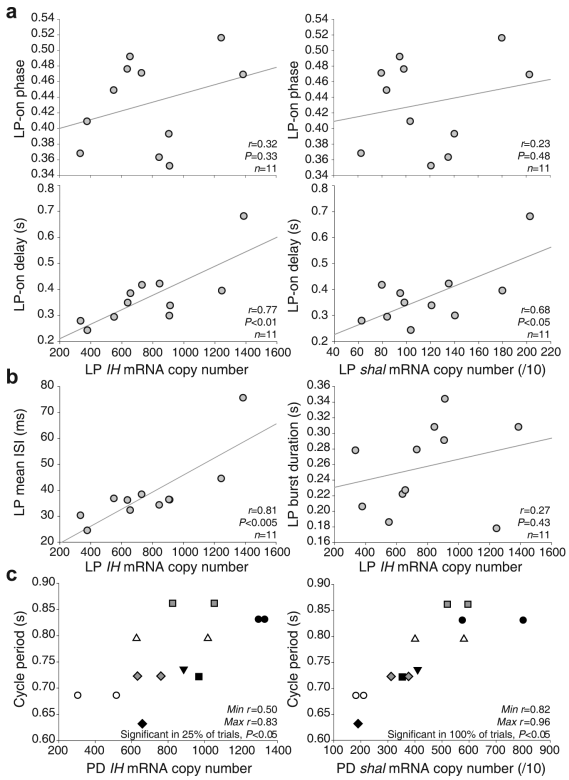

Figure 5.

Correlations between mRNA expression and network output. **(a)** *IH* and *shal* expression in LP were significantly correlated with LP-on delay (bottom panels) but not with LP-on phase (top panels). In all panels, gray line is a linear fit with *x* as the independent variable, *r* is the sample correlation coefficient, and P-value is from a test of the null hypothesis that the true correlation coefficient is zero (see Methods). **(b)** *IH* expression in LP was significantly correlated with mean LP ISI (left panel) but not with LP burst duration (right panel). **(c)** *IH* expression in PD was not significantly correlated with pyloric period (left panel), but *shal* expression in PD was (right panel). Data points with the same symbol are from the same animal (there are two PD cells per animal). Unpaired symbols are from animals for which expression levels could only be measured in one PD. Statistical analysis was performed after arbitrarily picking a single PD from each pair (identical symbols, with identical *y* values), leading to 32 (2^5) replications (see text). Maximum and minimum sample correlation coefficient values obtained across 32 replications are indicated (Max *r*, Min *r*). Percentage gives the fraction of the 32 replications for which a significant correlation was found ($P<0.05$).

Table 1

Correlations between synaptic properties, I_{MI} properties, channel expression, and firing properties in the LP and PD neurons.

CORRELATION	Sample correlation coefficient	*n*	*P value*
FIRING PROPERTIES (LP)			
Period ***vs*** LP-on delay	**0.85**	69	**<0.001**
Period ***vs*** mean LP ISI	**0.78**	69	**<0.001**
Period ***vs*** LP burst duration	**0.73**	69	**<0.001**
LP-on delay ***vs*** mean LP ISI	**0.75**	69	**<0.001**
SYNAPTIC PROPERTIES (LP)			
Erev ***vs*** Max gAB	**0.77**	22	**<0.001**
Erev ***vs*** Max gPD	− **0.90**	22	**<0.001**
Max gAB ***vs*** Max gPD	−0.46	22	<0.05
Max gPD ***vs*** Phase of Max gABPD	**0.57**	22	**<0.01**
Max gABPD ***vs*** Phase of Max gABPD	0.43	22	<0.05
SYNAPTIC vs FIRING (LP)			
Max gAB ***vs*** LP-on phase	−0.45	22	<0.05
Max gPD ***vs*** LP-on phase	**0.77**	22	**<0.001**
(gAB-gPD) ***vs*** LP-on phase	− **0.68**	22	**<0.001**
Phase of Max gABPD ***vs*** LP-on phase	**0.62**	22	**<0.005**
SYNAPTIC *vs* I_{MI} (LP)			
Max gPD ***vs*** Peak I_{MI}	0.56	15	<0.05
Phase of Max gABPD ***vs*** Peak I_{MI}	0.64	15	<0.05
I_{MI} vs FIRING (LP)			
Peak I_{MI} ***vs*** LP-on phase	**0.75**	15	**<0.005**
CHANNEL EXPRESSION *vs* FIRING (LP)			
IH ***vs*** mean LP ISI	**0.81**	11	**<0.005**
IH ***vs*** LP-on delay	0.77	11	<0.05
IH ***vs*** cycle period	0.69	11	<0.05
shal ***vs*** mean LP ISI	**0.75**	11	**<0.01**
shal ***vs*** LP-on delay	0.68	11	<0.05
shal ***vs*** cycle period	0.63	11	<0.05
shaw ***vs*** mean LP ISI	0.69	10	<0.05
shaw ***vs*** LP-on delay	0.63	10	<0.05
shab ***vs*** mean LP ISI	0.66	10	<0.05
CHANNEL EXPRESSION *vs* FIRING (PD)			
shal ***vs*** *cycle period (all cells included)*	**0.87**	13	**<0.001**

Abbreviations: Erev, composite synaptic reversal potential; phase of max gABPD, phase of maximum composite synaptic conductance; peak I_{MI}, absolute value of peak I_{MI} current amplitude; mean LP ISI, mean LP interspike interval. Sample correlation coefficients and P-values in bold indicate the most significant correlations.